This is a manuscript of an article from *Journal of Structural Engineering*, July 2014. Doi: 10.1061/(ASCE)ST.1943-541X.0001151. Posted with permission.

Dynamic Characterization of a Soft Elastomeric Capacitor for Structural Health Monitoring

Simon Laflamme [1], A.M. ASCE, Filippo Ubertini [2] , Hussam Saleem [3] , Antonella D'Alessandro [4]
Austin Downey [5] , Halil Ceylan [6] , Annibale Luigi Materazzi [7]

ABSTRACT

Structural health monitoring of civil infrastructures is a difficult task, often impeded by the geometrical size of the monitored systems. Recent advances in conducting polymers enabled the fabrication of flexible sensors capable of covering large areas, a possible solution to the monitoring challenge of mesoscale systems. The authors have previously proposed a novel sensor consisting of a soft elastomeric capacitor (SEC) acting as a strain gauge. Arranged in a network configuration, the SECs have the potential to cover very large surfaces. In this paper, we further the understanding of the proposed sensor by evaluating its performance at vibration-based monitoring of large-scale structures. The dynamic behavior of the SEC is characterized by subjecting the sensor to a frequency sweep, and detecting vibration modes of a full-scale steel beam. Results show that the sensor can be used to detect fundamental modes and dynamic input. Also, a network of SECs is used for output-only modal identification of a full-scale concrete beam, and results are benchmarked against off-the-shelf accelerometers. The SEC network performs well at estimating both natural frequencies and mode shapes. The resolution of the sensor is currently limited by the available electronics to measure small changes in capacitance, which reduces its accuracy with increasing frequencies in both the time and frequency domain.

Keywords: Soft elastomeric capacitor, smart sensors, nanotechnology, strain gauges, structural health monitoring, vibration signatures

INTRODUCTION

Structural health monitoring (SHM) of civil structures is the automation of the damage diagnosis, localization, and prognosis tasks. Successful SHM has the potential of enabling timely inspection and maintenance, resulting in enhanced structural safety and longer life span (Brownjohn 2007; Harms et al. 2010). However, SHM is difficult, because the monitored structures are typically geometrically large and complex. Off-the-

[1]Department of Civil, Construction, and Environmental Engineering, and Department of Electrical and Computer Engineering, Iowa State University, Ames, IA, 50011, corresponding author; email: laflamme@iastate.edu, phone: (515) 294-3162.
[2]Department of Civil and Environmental Engineering, University of Perugia, Via G. Duranti 93, Perugia 06125, Italy
[3]Department of Civil, Construction, and Environmental Engineering, Iowa State University, Ames, IA 50011, USA
[4]Department of Civil and Environmental Engineering, University of Perugia, Via G. Duranti 93, Perugia 06125, Italy
[5]Department of Civil, Construction, and Environmental Engineering, Iowa State University, Ames, IA 50011, USA
[6]Department of Civil, Construction, and Environmental Engineering, Iowa State University, Ames, IA 50011, USA
[7]Department of Civil and Environmental Engineering, University of Perugia, Via G. Duranti 93, Perugia 06125, Italy

shelf sensing solutions offer great precision and operability, but are hardly scalable without necessitating substantial costs and complex signal processing algorithms, resulting in SHM being less attractive on an investment point of view.

The authors have developed a novel sensor specifically dedicated to SHM of mesosystems (Laflamme et al. 2012b). The sensor is a flexible skin constituted from an array of soft elastomeric capacitors (SECs), each acting as a large-scale strain gauge transducing changes in strain into changes in capacitance. An SEC is fabricated from a styrene-ethylene-butylene-styrene (SEBS) matrix mixed with titanium dioxide (TiO_2 or titania) sandwiched between electrode plates composed of SEBS mixed with carbon black (CB). The typical dimension of a single SEC is approximately 75×75 mm^2, but its size and shape can be customized.

Sensors fabricated from flexible electronics have been previously proposed and studied for SHM applications (Hurlebaus and Gaul 2004; Carlson et al. 2006; Tata et al. 2009; Mohammad and Huang 2010; Jang and Kim 2012). Several studies use carbon nanotubes particles to create resistance-based sensors (Kang et al. 2006; Loh et al. 2009; Gao et al. 2010; Srivastava et al. 2011). Capacitance-based strain sensors have also been proposed, where a flexible dielectric is created by incorporating nanoparticles of high dielectric permittivity within the polymer. Applications of capacitance-based flexible sensors include strain (Arshak et al. 2000; Suster et al. 2006), pressure (Lipomi et al. 2011), tri-axial force (Dobrzynska and Gijs 2013), and humidity (Harrey et al. 2002; Hong et al. 2012) gauges. The SEC developed by the authors differs from literature by combining a large physical size, relatively high initial capacitance, and high mechanical robustness, resulting in a larger surface coverage and higher sensitivity. Arranged in a network configuration, the SECs can cover mesosurfaces at low cost, operate at low frequencies, and consume low power.

The concept of SHM using large SECs has been demonstrated by the authors using an off-the-shelf thin film capacitor (Laflamme et al. 2012a), and with the nanoparticle mix used in this paper (Laflamme et al. 2012b). The static characterization of the sensor is discussed in (Laflamme et al. 2013). In this paper, we study the performance of the SEC at dynamic monitoring of civil structures.

The paper is organized as follows. The upcoming section presents the background theory on the SEC, including the fabrication process, the electromechanical model and the static behavior. Subsequently, the dynamic behavior of the sensor is characterized under a sweeping harmonic input. Tests are conducted on a single SEC in a bending mode, and on a large-scale steel beam. Thereafter, the performance of a network of SECs at detecting modal characteristics is studied. Tests are conducted on a large-scale concrete beam and results from the SECs are benchmarked against results from off-the-shelf accelerometers. The last section discusses the results and concludes the paper.

BACKGROUND

Sensor Fabrication

Synthetic metals typically originate from the constitution of a nanocomposite mix of organic and inorganic particles, which can be obtained via chemical and electromechanical preparations (Gangopadhyay and De 2000). The challenge in the fabrication of an SEC for mesosensing lies in the selection of an inexpensive mix that would be chemically and mechanically robust over time and exposure to harsh environments. The dielectric of the SEC is composed of an SEBS matrix, a block copolymer used in many medical applications due to their purity, softness, elasticity, and strength (Yoda 1998), filled with titania, an inorganic particle characterized by a high dielectric permittivity that increases the permittivity and durability of the polymer (Stoyanov et al. 2010). The electrodes are fabricated using the same organic matrix, but this time filled with CB to create conducting plates. These CB particles are selected due to their high conductivity and low cost. The utilization of the same polymer matrix for both the electrodes and dielectric ensures a strong mechanical bond between layers.

An SEC is fabricated using a drop-cast process, shown in Fig. 1. First, the SEBS (Mediprene Dryflex) particles are dissolved in toluene (Fig. 1(a)). The solution is doped with TiO_2 rutile (Sachtleben R 320 D) by dispersing a 15% vol. concentration using an ultrasonic tip (Fisher Scientific D100 Sonic Dismembrator) (Fig. 1(b)). The SEBS-TiO_2 solution is drop casted on an 75×75 mm^2 glass slides and dries for 48 hours to allow the toluene to evaporate (Fig. 1(c)). While drying occurs, a 10% vol. concentration of CB (Printex XE 2-B) is added to another SEBS-toluene solution. The CB particles are dispersed in a sonic bath over 24 hours (Fig. 1(d)), resulting in a conducting solution. This solution is painted onto the top and bottom surfaces of the dried dielectric to create the electrode plates, and let drying for 48 hours to allow the toluene to evaporate. Two conductive copper tapes are embedded into the liquid electrode mix during the drying process to create mechanical connections for the wires linking the sensor to the data acquisition system. It is worth noting that these copper tapes could be replaced by different conductive tapes or direct integration of wireless communication circuitry. Fig. 1(f) is a picture of a typical SEC resulting from this fabrication process. Fig. 2 is a scanning electron microscope (SEM) picture of an SEC showing a uniform dispersion of the titania particles. It is also possible to use a melt-mixing process to fabricate an SEC, which eliminates the solvents from the process, but further complicates the dispersion of the titania (Saleem et al. 2013).

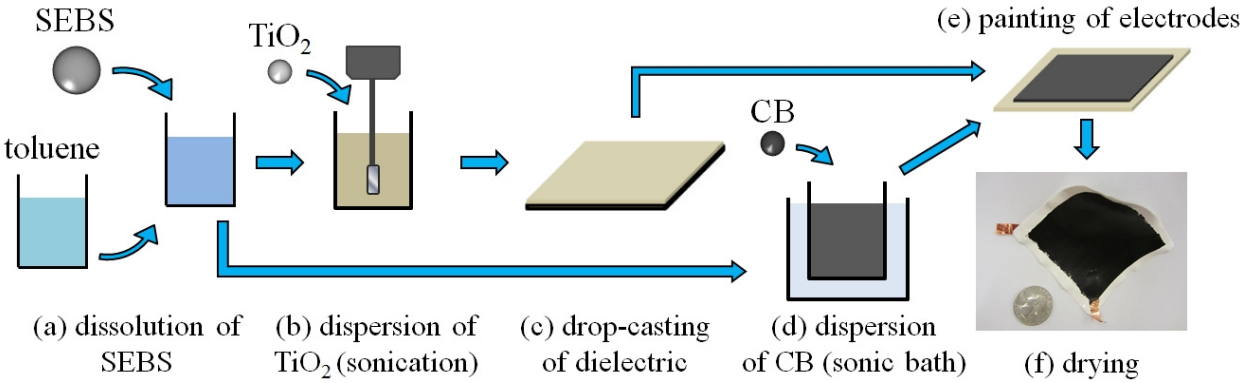


FIG. 1. Fabrication process of an SEC.

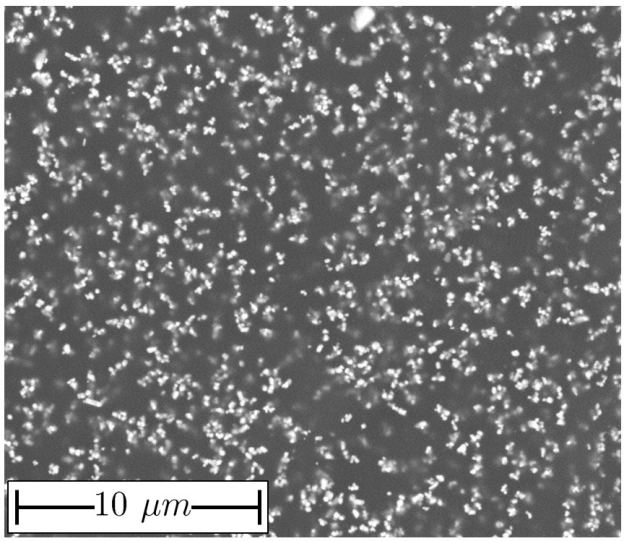


FIG. 2. SEM picture of an SEC.

Electromechanical Model

Fig. 3 illustrates the sensing principle for an SEC wired to a data acquisition system (DAQ), showing the principal strains ε_x, ε_y, or ε_z. A change in strain over the sensing materials is converted into a change in capacitance ΔC which can be directly measured by the DAQ. In monitoring of surface strain, the SEC is adhered onto the surface using an epoxy in the $x-y$ plane, and it is assumed that no external force acts along the vertical axis z. Using Hooke's Law under plane stress assumption, ε_z can be written as a function of ε_x and ε_y:

$$\varepsilon_z = -\frac{\nu}{1-\nu}(\varepsilon_x + \varepsilon_y) \tag{1}$$

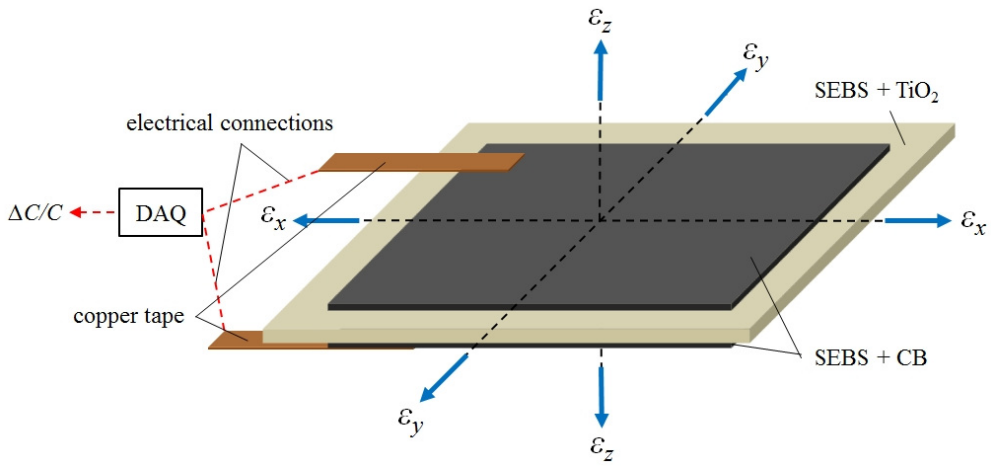


FIG. 3. Sensing principle (layers not scaled).

Also, the SEC measured a low frequencies (< 1000 Hz) can be approximated as a non-lossy capacitor C:

$$C = e_0 e_r \frac{A}{h} \tag{2}$$

where $e_0 = 8.854$ pF/m is the vacuum permittivity, e_r the dimensionless polymer relative permittivity, $A = w \cdot l$ the sensor area with width w and length l, and h the height of the dielectric. Assuming small changes in C, the differential of Eq. (2) leads to an expression relating strain to a change in capacitance ΔC:

$$\begin{aligned} \Delta C &= \left(\frac{\Delta l}{l} + \frac{\Delta w}{w} - \frac{\Delta h}{h} \right) C \\ \frac{\Delta C}{C} &= \varepsilon_x + \varepsilon_y - \varepsilon_z \end{aligned} \tag{3}$$

Using the expression for ε_z from Eq. (1) into Eq. (3) gives an expression for the gauge factor

$$\frac{\Delta C}{C} = \frac{1}{1-\nu}(\varepsilon_x + \varepsilon_y) \tag{4}$$

with the gauge factor equal to $1/(1-\nu)$. Here, the SEC materials can be approximated as incompressible (the poisson ratio of pure SEBS $\nu \approx 0.49$ (Wilkinson et al. 2004)):

$$\frac{\Delta C}{C} = 2(\varepsilon_x + \varepsilon_y) \tag{5}$$

which gives a gauge factor of 2. It follows from Eq. (5) that a possible disadvantage of the SEC is that the

sensor' signal corresponds to the additive strain in both x- and y-directions. A strategy to cope with this issue is to utilize a matrix of sensors, and exploit geometry and correlation to decompose the signal into both principal strain components. The authors are currently developing algorithms to address this shortcoming. In the proposed utilization for dynamic monitoring, this bi-directional measurement turns into an advantage, where the sensor can detect modal properties in all directions.

Eq. (5) can be specialized for a uniaxial strain along the x-axis where $\varepsilon_y = -\nu_m \varepsilon_x$, with ν_m being the Poisson's ratio of the monitored material assumed to be significantly stiffer than the SEC:

$$\frac{\Delta C}{C} = \frac{1-\nu_m}{1-\nu}\varepsilon \tag{6}$$

or for a free-standing sensor (not bonded) undergoing uniaxial strain ($\sigma_y = 0$, $\varepsilon_y = -\nu\varepsilon_x$, $\varepsilon_x = \varepsilon$):

$$\frac{\Delta C}{C} = \varepsilon \tag{7}$$

which reduces the gauge factor to 1. Assuming that the Poisson ratio is mostly defined by the SEBS matrix, the gauge factor is approximatively independent on the inorganic particles. However, the sensitivity of the sensor $\Delta C/\varepsilon$ is directly dependent on the dielectric permittivity and sensor geometry. The sensitivity can be increased by decreasing the SEC thickness, increasing the width, or increasing the dielectric permittivity, which is attained by altering the nanocomposite mix (Kollosche et al. 2011).

DYNAMIC CHARACTERIZATION

The dynamic characterization of the SEC is initiated by evaluating the performance of a single sensor at detecting structural dynamic signatures. This is done by investigating the capacity of an SEC at detecting a particular frequency input. This series of tests is conducted on a small cantilever steel beam subjected to a dynamic load using an Instron 8801 servohydraulic testing system. The beam dimensions are $300 \times 100 \times 12.5\,\mathrm{mm}^3$, giving an analytical fundamental frequency of 25.2 Hz, which is similar to the dominant frequency of the large-scale steel beam used for the full-scale verification. An SEC is installed onto the surface of the beam 63.5 mm from the fixed end. The excitation is applied 165 mm from the fixed end in the center, and consists of a sweeping harmonic from 1 to 40 Hz with 1 Hz increments. The SEC capacitance is acquired using an ACAM PCAP01 DAQ sampled at 145 Hz, and the load input is acquired directly from the Instron at 160 Hz. Fig. 4 shows the experimental setup. The SEC measures surface strain, and measurements are benchmarked against analytical strain computed from the actuator force using the Euler-Bernoulli beam theory.

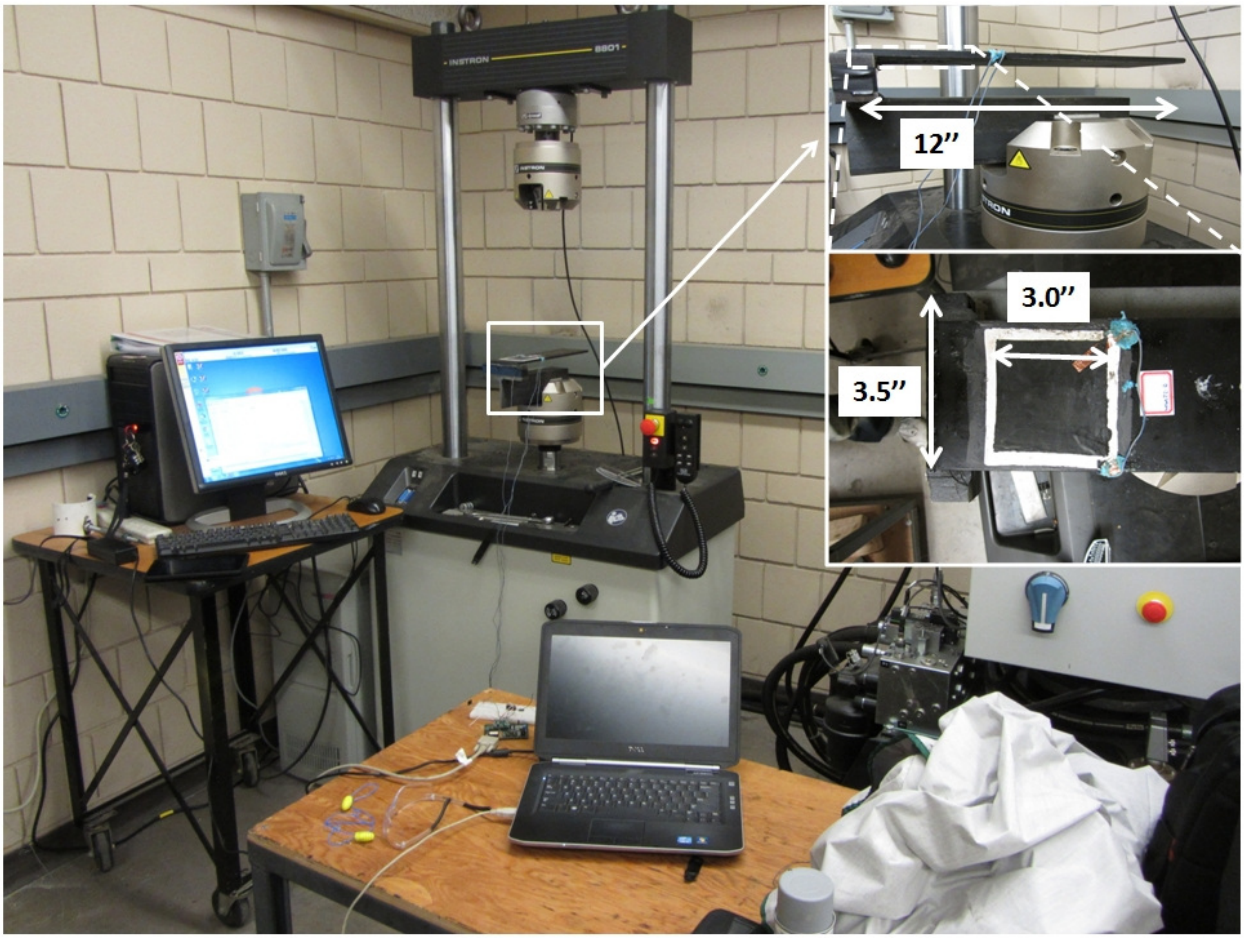


FIG. 4. Laboratory setup - small scale beam.

Fig. 5 is a plot of the typical raw signal from the SEC at 1, 10 and 20 Hz. There is a drift in the signal that can be observed by comparing the average capacitance values between each subfigures. This drift in the signal is linear, and may be caused by the capacitance measurement method from the DAQ. Further investigations on this linear drift will be needed. A comparison between the signals shows that the noise-to-signal ratio increases with increasing frequency. This is also observed in the wavelet decomposition shown in Fig. 6. The wavelet transform has been obtained using morlet wavelet, normalized at each discrete time interval to the highest wavelet amplitude. The frequency sweep input, indicated by the black stair-steps line, is clearly identified by the wavelet transform, but the noise-to-signal ratio increases with frequency due to the presence of white noise that becomes significant with respect to the SEC measurements.

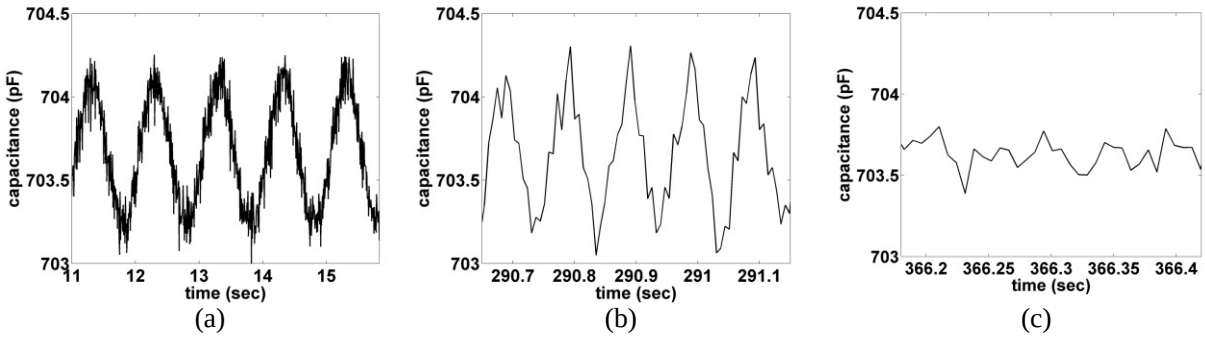


FIG. 5. SEC capacitance signal at (a) 1 Hz; (b) 10 Hz; and (c) 20 Hz.

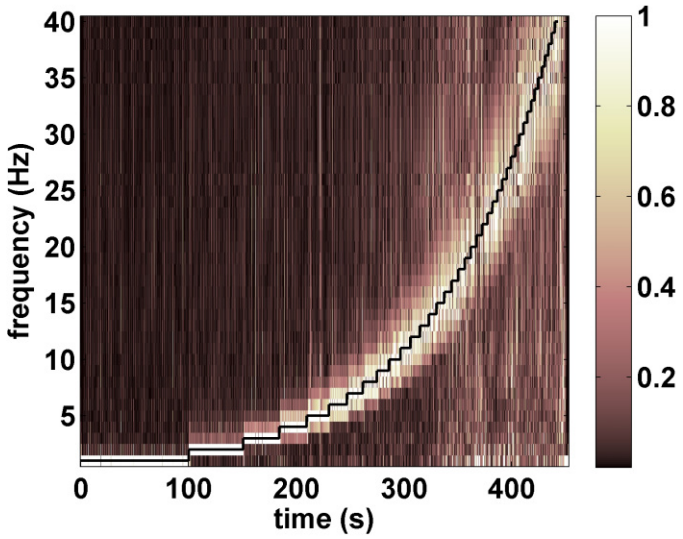


FIG. 6. Normalized wavelet decomposition of the output signal - small scale beam.

Fig. 7 compares the time series of the measured strain using Eq. (6) and the analytical strain using the Euler Bernoulli beam theory. A noticeable feature in the signal is the reduction in the peak strain response of the SEC with increasing frequency, a phenomenon attributed to the strain-rate dependency of the SEBS (Stoyanov et al. 2010), as well as an adiabatic heating effect causing the bonds to soften (Arruda et al. 1995). Constitutive models for elastomeric materials have been developed to characterize this strain dependency; see Refs. (Bergström and Boyce 2000; Amin et al. 2006; Richeton et al. 2006; Bhuiyan et al. 2009; Razzaq et al. 2010) for instance. The characterization of the material rheology is out of the scope of this paper. This reduction in peak strain is also observed in the sensor's frequency response. Fig. 8(b) shows the SEC frequency response function (FRF) plot obtained by dividing the fourier transform of the measured strain by the analytical strain input (Fig. 8(a)), obtained after windowing of the signal using a Tukey window to reduce frequency leakage. The FRF plot shows a transfer function close to unity for frequencies below 14

Hz, but starts to decrease beyond this point. Fig. 8(b) only shows the FRF for up to 20 Hz; data beyond this point contain a relatively high level of noise, as shown in the zoom of Fig. 8(a), which impedes a precise computation of the FRF. One can conclude that the performance of the SEC in the time domain is limited to approximately 15 Hz. Despite such limitation, likely attributed to limitations in the DAQ, the Fourier transform (Fig. 8(a)) shows that the sensor can detect the frequency input over the range 1-40 Hz, useful for vibration-based monitoring.

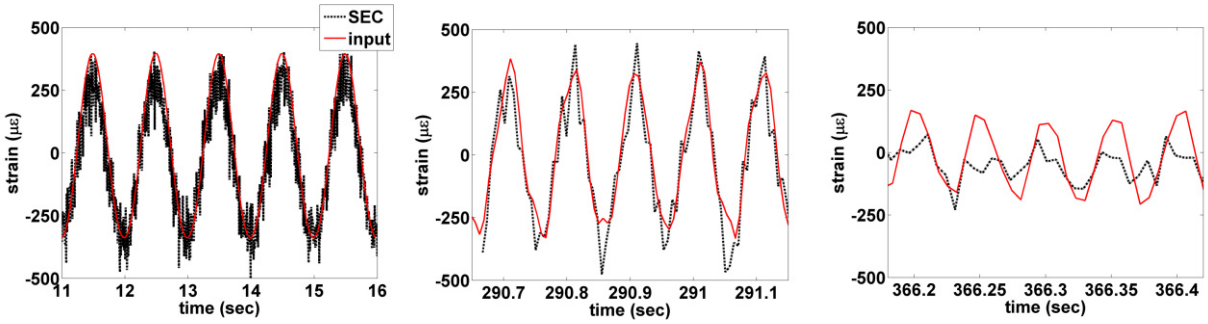


FIG. 7. Measured versus analytical strain at (a) 1 Hz; (b) 10 Hz; and (c) 20 Hz.

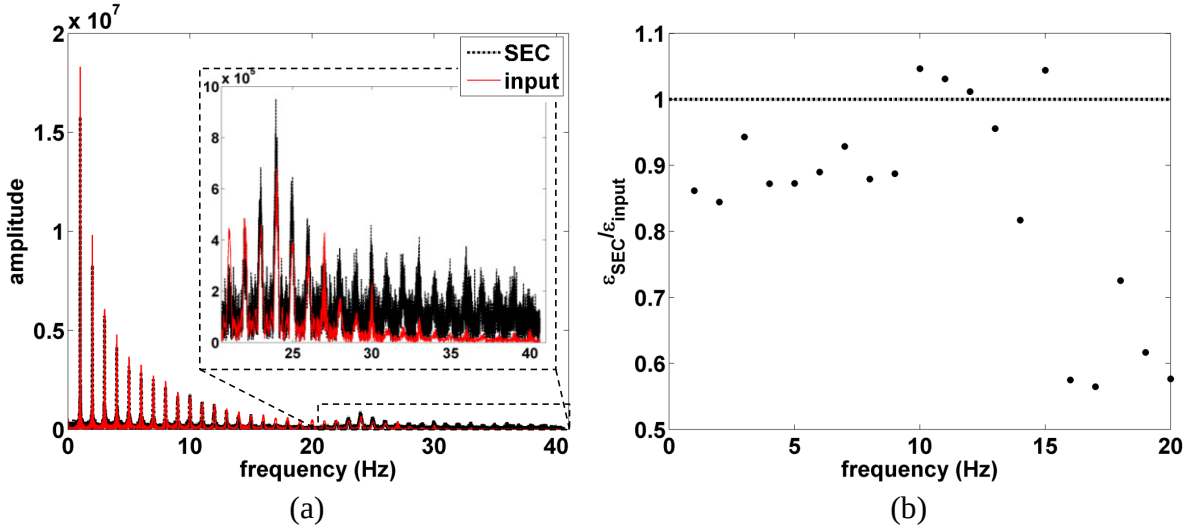


FIG. 8. (a) Fourier transforms of the analytical and measured strain signals; and (b) FRF.

Validation on Full-Scale Beam

Results discussed above are validated on a full-scale steel beam, where the SEC is used to detect natural frequencies. This test has been conducted earlier, when the version of the DAQ used above was not yet available. Here, the first generation of the ACAM DAQ system (PICOAMP PSØ21) was used, which only

allowed the measurement of a single capacitance via the differential measurement between two capacitors. For this reason, two SECs were used in the experiment in a differential measurement mode. The SECs were deployed on a 5.5 m HP10x42 simply supported steel beam, at a distance of 280 mm from each other, 1.8 m from the left support, as shown in Fig. 9. The beam was excited using a 4000 rpm capacity shaker, installed on the top flange of the beam to produce a dynamic load along the strong axis of the beam, at 2.85 m from the left support (Fig. 9). A chirp signal was generated manually and the signal from the SECs acquired over 35 seconds and sampled at 200 Hz.

A plot of the power spectral density (PSD) is shown in Fig. 10. Results from the test are benchmark against a finite element model (FEM) of the beam created in SAP2000. Table 1 compares results obtained from the PSD and the FEM. The SECs were capable of detecting all six modes, in good agreement with the FEM model, regardless of the excited axis. Given the success of this initial test, the next stage was to compare the performance of the SECs in a network configuration, against off-the-shelf accelerometers. This additional test is described in the following subsection.

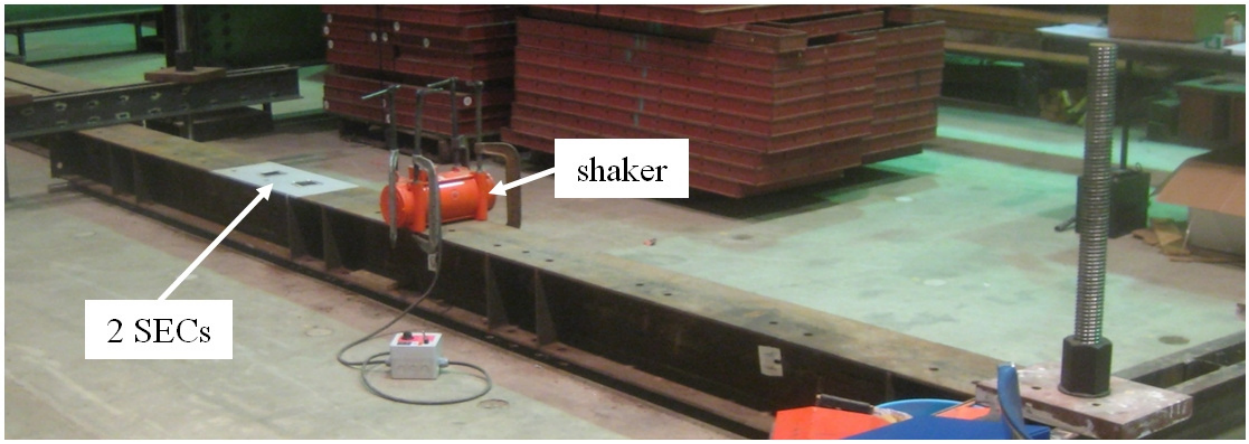


FIG. 9. Laboratory setup - full-scale beam.

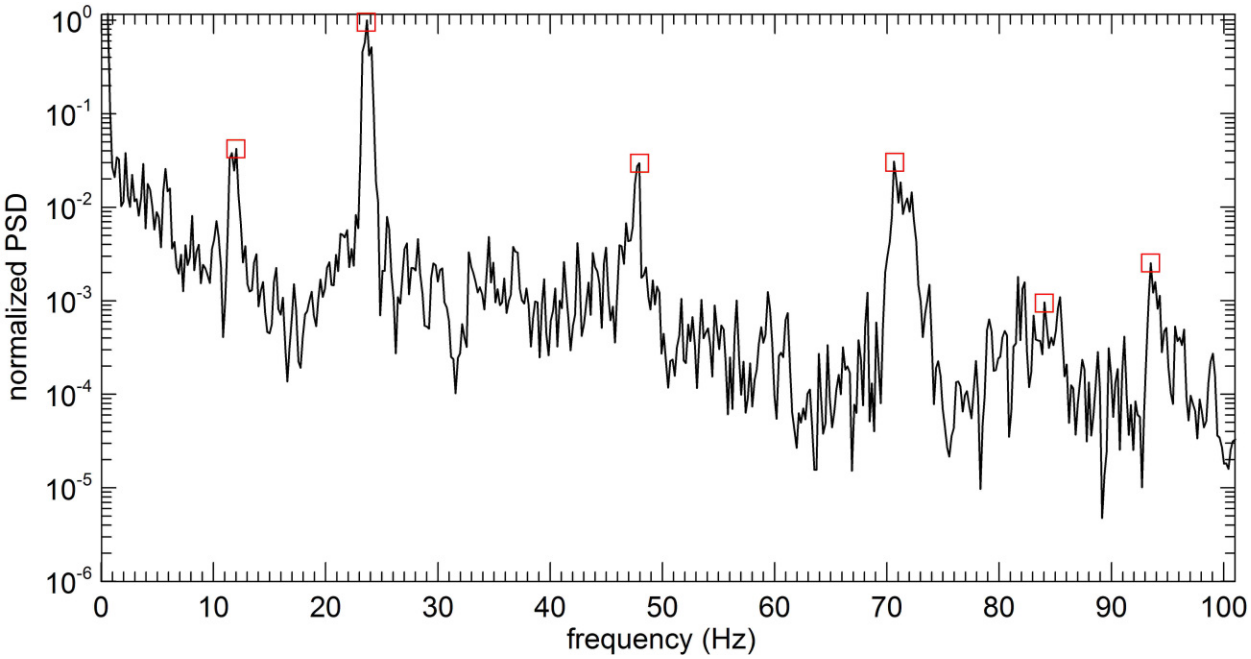


FIG. 10. Power spectral density plot with peak selection for identification of modal frequencies.

TABLE 1. Modal frequency identification - full-scale beam.

	mode number (mode axis)					
	1 (weak)	2 (torsion)	3 (strong)	4 (weak)	5 (torsion)	6 (strong)
FEM (Hz)	12.3	26.5	42.9	65.8	91.3	117.0
SEC (Hz)	11.8	23.9	47.4	71.1	83.5	94
difference (%)	-4.07	-9.81	10.5	8.05	-8.54	-19.7

Fig. 11 shows a wavelet transform of the sensor signal obtained using the same signal processing technique as described earlier. Results from Fig. 11 shows the ramping frequency input. One feature in the plot is the plateau at 23.9 Hz. This is the fundamental frequency of the torsional mode, which resonates between 21 and 24 seconds. A second feature is the ramping frequency in the lower middle of the plot. This feature can be explained by a second excitation produced by the shaker in the perpendicular direction, exciting the weak axis of the beam, which can also be measured by the sensor given its bi-directional measurement capability.

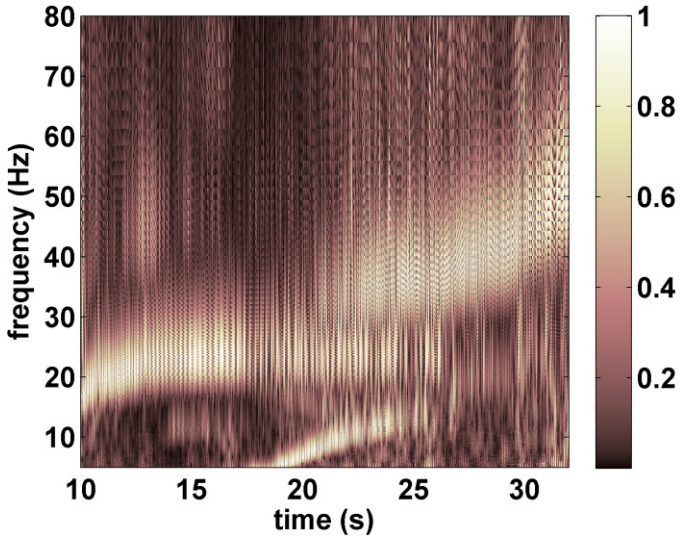


FIG. 11. Normalized wavelet decomposition of the output signal - full-scale beam.

OUTPUT-ONLY MODAL IDENTIFICATION

Experimental setup

This series of tests has been conducted using the second generation of the capacitance DAQ from ACAM (PCAP01). This particular off-the-shelf DAQ enabled the measurement of multiple capacitors in differential mode (seven different capacitors) using an additional capacitor for the differential readings. This new DAQ allowed the utilization of the SECs in a network configuration for modal identification. The test consisted of deploying three SECs over a full-scale reinforced concrete beam located inside a laboratory. The tests focused on the range of frequencies from 0 to 200 Hz, covering a wide range of natural frequencies found in typical civil structures. The beam was excited using an impact hammer, and its response measured and recorded simultaneously with the SECs. Results are benchmarked against those obtained through an array of seven equally spaced accelerometers. The layout of the sensors is shown in Fig. 12.

The RC beam has dimensions of $200 \times 300 \times 4000$ mm^3, and is equipped with two steel plates partially embedded at its extremities prior to casting, serving as vertical supports. The plates are inserted into steel supports to allow end rotations in the vertical plane while fixing rotations in the horizontal plane. The analytical vertical fundamental frequencies of the first three modes (denoted as V1, V2 and V3) are 25.2 Hz, 100.9 Hz and 227 Hz, respectively.

Seven accelerometers (PCB393C - 1 V/g sensitivity with ± 2.5 g measurement range) $A1$ through $A7$ were attached through permanent magnets onto $40 \times 40 \times 8$ mm^3 steel plates that were glued onto the beam. The accelerometers were wired to the central unit by means of short coaxial cables. SECs S1, S2, and S3

were glued over the beam at the locations corresponding to accelerometers A2, A3 and A4.

The beam was excited with an impulse hammer (PCB 086D20C41) using random hits in space and time. The outputs of accelerometers were acquired through an 8 channels data acquisition module, model PXIe-4492 (24-bit resolution with anti aliasing filters), installed in a PXIe-1073 platform. Data sampling rates and durations were beyond the Nyquist sampling rate and significantly larger than the first structural periods, respectively, which allowed an accurate frequency identification. The outputs of the SEC were sampled at 440 Hz.

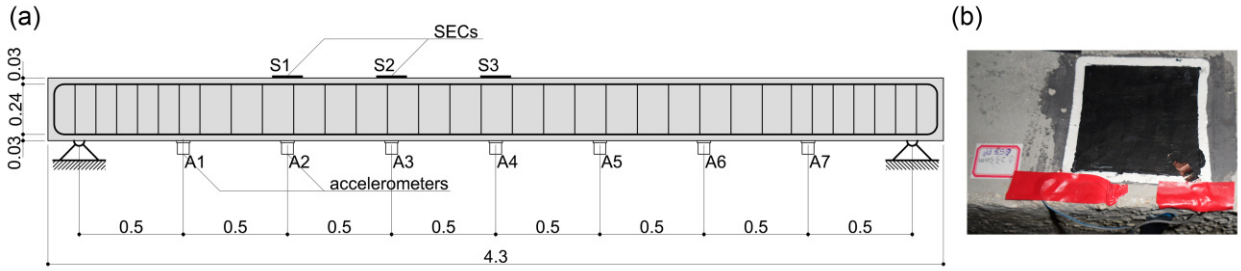


FIG. 12. Experimental setup for tests on RC beam: (a) sensors layout and elevation of the investigated beam (dimensions in inches); and (b) SEC glued onto the beam.

Data analysis and results

Classic canonical variate analysis of stochastic subspace identification (SSI) (Van Overschee and De Moor 1996) is employed for data analysis, because of its known performances in output only modal identification. An automated modal identification procedure based on clustering analysis is also used to automatically interpret the results of SSI and provide modal parameters estimates (Ubertini et al. 2013).

Modal parameters of the RC beam were first estimated using accelerometers outputs and clustering analysis. These results provided four vertical modes, denoted by V1, V2A, V2B, V3, in the range 0-200 Hz. Modes V2A and V2B have very similar associated mode shapes, corresponding to the lowest antisymmetric mode of the beam, but different frequencies. They probably originate from a splitting of the second mode due to cracking of the beam. The analysis of the data recorded in a test with accelerometers placed in the lateral direction also highlighted the presence of three lateral modes within the 0-200 Hz range, L1, L2 and L3, with the addition of two low frequency lateral modes associated with movements of the supports and denoted LS1 and LS2.

The capability of SECs to detect fundamental modes of the RC beam is evaluated, at first, using stabilization diagrams (SDs). This type of plots is very popular and often used in literature to discriminate structural modes identified via SSI from spurious noise modes associated to noise in measurements and overmodeling effects. They constitute plots of stable (or consistent) poles in an order-frequency plane. Stability of poles is

evaluated by comparing the identified frequencies, damping ratios and mode shapes from models of orders n and $n+2$, and determining the consistency of poles. Vertical alignments of stable poles highlight the modes whose properties do not change significantly when varying the dimension of the state vector, likely corresponding to structural modes. Conversely, spurious noise modes do not usually appear consistently for varying the model order.

The SDs of the outputs from the three SECs and three accelerometers placed at the same locations as the SECs are shown in Fig. 13. Consistent poles are denoted by a black star, while a pole that only satisfies frequency and mode shape similarity is denoted by a gray triangle. Modal frequencies identified from clustering analysis are indicated with vertical lines.

Fig. 13 shows that the SDs of SECs and accelerometers' outputs are very similar, showing almost the same vertical alignments, which mostly correspond to the modes identified via clustering analysis of all acceleration data. Some lateral modes, such as LS1, are clearly visible in the SD of SECs but not on that of accelerometers, demonstrating the capability of SECs to sense strain in two orthogonal directions. Results generally confirm the ability of SECs to detect structural modes. Some differences in frequencies of modes identified from accelerometers and SECs are conceivably caused by a variation in temperature in the laboratory, as both sets of measurements were performed independently to reduce electromagnetic noise. Other vertical alignments, not corresponding to estimated modes, are also visible in both SDs and probably associated with residual spurious modes that can be eliminated via clustering analysis.

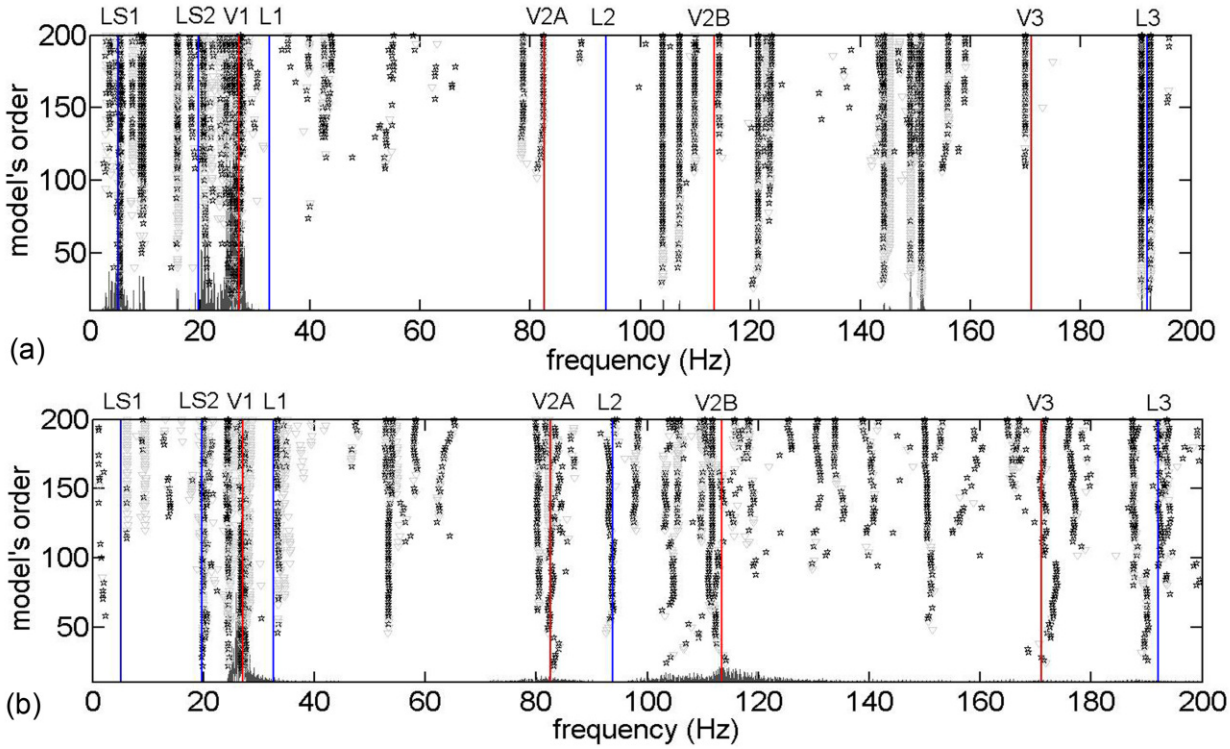


FIG. 13. SDs of SECs ouptuts (a) and accelerometers data (b) (vertical lines denote the modes identified from clustering analysis of the data recorded by all accelerometers).

The mode shapes identified through clustering analysis from the SECs outputs and all accelerometers outputs are compared in Fig. 14. Mode V2A is not shown in these results because it was not clearly identified by the SECs. The other vertical mode shapes identified by the SECs appear to be in good agreement with those of the accelerometers, with high values of the modal assurance criterion (MAC). Larger differences are observed in the second mode (V2B) and can be explained by a lower level of modal excitation and an insufficient resolution of the DAQ.

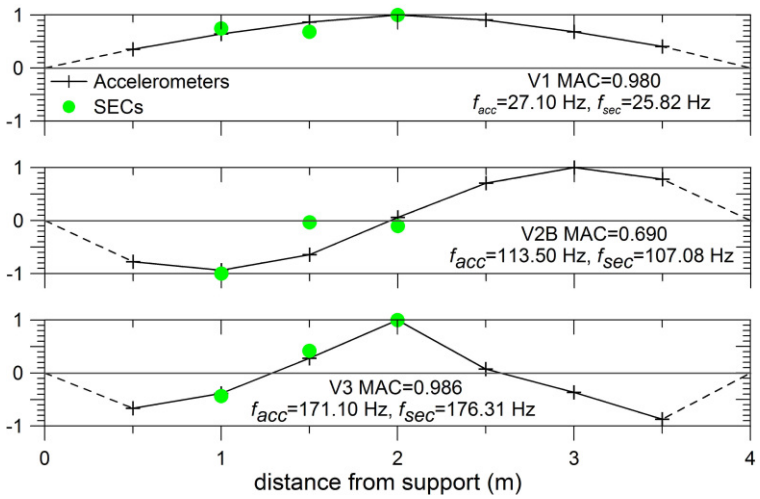


FIG. 14. Mode shapes identified from clustering analysis using SECs and accelerometers.

CONCLUSION

The dynamic behavior of a novel thin film sensor for strain sensing of mesosystems has been characterized. The sensor consists of a thin film polymer fabricated using inexpensive organic and inorganic particles. The particular mix of SEBS and titania constituting the sensor provides mechanical robustness and good sensitivity to strain.

Results show that the sensor was capable of detecting frequency inputs in the range 1-40 Hz, but the presence of noise, likely arising from the DAQ, showed that the SEC was limited below 15 Hz in the time domain. Both full-scale tests conducted on steel and concrete specimens concluded that the sensor was capable of detecting fundamental frequencies up to 200 Hz, comparing well against analytical solutions and off-the-shelf accelerometers. A notable feature of the sensor was its capacity to detect modes in any directions, a consequence of the sensor's bi-directional measurements, which constitutes a great advantage over some of the existing sensing solutions. Lastly, results showed that the SEC could be used in a network configuration to identify mode shapes.

Progress in the electronics has the potential to substantially improve on the sensor's resolution and accuracy. Given the inexpensive scalability of the proposed sensing solution, along with the bi-directional sensing capability, the SEC constitutes a promising sensor for dynamic monitoring of civil structures by deploying large network of sensors over the monitored surfaces.

ACKNOWLEDGMENTS

This work is partly supported by the Iowa State University Council on International Programs, grant 1001062565 from the Iowa Alliance for Wind Innovation and Novel Development (IAWIND), and grant 13-02 from the Iowa Energy Center; their support is gratefully acknowledged.

REFERENCES

Amin, A., Lion, A., Sekita, S., and Okui, Y. (2006). "Nonlinear dependence of viscosity in modeling the rate-dependent response of natural and high damping rubbers in compression and shear: Experimental identification and numerical verification." International Journal of Plasticity, 22(9), 1610–1657.

Arruda, E. M., Boyce, M. C., and Jayachandran, R. (1995). "Effects of strain rate, temperature and thermomechanical coupling on the finite strain deformation of glassy polymers." Mechanics of Materials, 19(2-3), 193–212.

Arshak, K., McDonagh, D., and Durcan, M. (2000). "Development of new capacitive strain sensors based on thick film polymer and cermet technologies." Sensors and Actuators A: Physical, 79(2), 102–114.

Bergström, J. and Boyce, M. (2000). "Large strain time-dependent behavior of filled elastomers." Mechanics of materials, 32(11), 627–644.

Bhuiyan, A., Okui, Y., Mitamura, H., and Imai, T. (2009). "A rheology model of high damping rubber bearings for seismic analysis: Identification of nonlinear viscosity." International Journal of Solids and Structures, 46(7), 1778–1792.

Brownjohn, J. (2007). "Structural health monitoring of civil infrastructure." Philosophical Transactions of the Royal Society A: Mathematical, Physical and Engineering Sciences, 365(1851), 589–622.

Carlson, J., English, J., and Coe, D. (2006). "A flexible, self-healing sensor skin." Smart materials and structures, 15, N129.

Dobrzynska, J. A. and Gijs, M. (2013). "Polymer-based flexible capacitive sensor for three-axial force measurements." Journal of Micromechanics and Microengineering, 23(1), 015009.

Gangopadhyay, R. and De, A. (2000). "Conducting polymer nanocomposites: a brief overview." Chemistry of Materials, 12(3), 608–622.

Gao, L., Thostenson, E., Zhang, Z., Byun, J., and Chou, T. (2010). "Damage monitoring in fiber-reinforced composites under fatigue loading using carbon nanotube networks." Philosophical Magazine, 90(31-32), 4085–4099.

Harms, T., Sedigh, S., and Bastianini, F. (2010). "Structural Health Monitoring of Bridges Using Wireless Sensor Networks." Instrumentation & Measurement Magazine, IEEE, 13(6), 14–18.

Harrey, P., Ramsey, B., Evans, P., and Harrison, D. (2002). "Capacitive-type humidity sensors fabricated using the offset lithographic printing process." Sensors and Actuators B: Chemical, 87(2), 226–232.

Hong, H. P., Jung, K. H., Min, N. K., Rhee, Y. H., and Park, C. W. (2012). "A highly fast capacitive-type humidity sensor using percolating carbon nanotube films as a porous electrode material." Sensors, 2012 IEEE, 1–4.

Hurlebaus, S. and Gaul, L. (2004). "Smart layer for damage diagnostics." Journal of intelligent material systems and structures, 15(9-10), 729–736.

Jang, S. D. and Kim, J. (2012). "Passive wireless structural health monitoring sensor made with a flexible planar dipole antenna." Smart Materials and Structures, 21(2), 027001.

Kang, I., Schulz, M. J., Kim, J. H., Shanov, V., and Shi, D. (2006). "A carbon nanotube strain sensor for structural health monitoring." Smart materials and structures, 15(3), 737.

Kollosche, M., Stoyanov, H., Laflamme, S., and Kofod, G. (2011). "Strongly enhanced sensitivity in elastic capacitive strain sensors." Journal of Materials Chemistry, 21(23), 8292–8294.

Laflamme, S., Kollosche, M., Connor, J., and Kofod, G. (2012a). "Soft capacitive sensor for structural health monitoring of large-scale systems." Structural Control and Health Monitoring, 19(1), 70–81.

Laflamme, S., Kollosche, M., Connor, J. J., and Kofod, G. (2012b). "Robust flexible capacitive surface sensor for structural health monitoring applications." Journal of Engineering Mechanics.

Laflamme, S., Saleem, H., Vasan, B., Geiger, R., Chen, D., Kessler, M., and Rajan, K. (2013). "Elastomeric capacitor network for strain sensing over large surfaces." IEEE/ASME Transactions on Mechatronics, 18(6), 1647–1654.

Lipomi, D. J., Vosgueritchian, M., Tee, B. C., Hellstrom, S. L., Lee, J. A., Fox, C. H., and Bao, Z. (2011). "Skin-like pressure and strain sensors based on transparent elastic films of carbon nanotubes." Nature nanotechnology, 6(12), 788–792.

Loh, K., Hou, T., Lynch, J., and Kotov, N. (2009). "Carbon nanotube sensing skins for spatial strain and impact damage identification." Journal of Nondestructive Evaluation, 28(1), 9–25.

Mohammad, I. and Huang, H. (2010). "Monitoring fatigue crack growth and opening using antenna sensors." Smart Materials and Structures, 19(5), 055023.

Razzaq, M., Bhuiyan, A., Okui, Y., Mitamura, H., and Imai, T. (2010). "Effect of rubber bearing's modeling on seismic response of base isolated highway bridge." 7th CUEE and 5th ICEE Joint Conference.

Richeton, J., Ahzi, S., Vecchio, K., Jiang, F., and Adharapurapu, R. (2006). "Influence of temperature and strain rate on the mechanical behavior of three amorphous polymers: Characterization and modeling of the compressive yield stress." International journal of solids and structures, 43(7), 2318–2335.

Saleem, H., Thunga, M., Kollosche, M., Kessler, M., and Laflamme, S. (2013). "Bio-inspired sensory membrane: Fabrication processes for full-scale implementation." AIP Conference Proceedings, Vol. 1511, 1601.

Srivastava, R. K., Vemuru, V. S. M., Zeng, Y., Vajtai, R., Nagarajaiah, S., Ajayan, P. M., and Srivastava, A. (2011). "The strain sensing and thermal–mechanical behavior of flexible multi-walled carbon nanotube/polystyrene composite films." Carbon, 49(12), 3928–3936.

Stoyanov, H., Kollosche, M., McCarthy, D. N., and Kofod, G. (2010). "Molecular composites with enhanced

energy density for electroactive polymers." Journal of Material Chemistry, 20, 7558–7564.

Suster, M., Guo, J., Chaimanonart, N., Ko, W. H., and Young, D. J. (2006). "A high-performance mems capacitive strain sensing system." Journal of Microelectromechanical Systems, 15(5), 1069–1077.

Tata, U., Deshmukh, S., Chiao, J., Carter, R., and Huang, H. (2009). "Bio-inspired sensor skins for structural health monitoring." Smart Materials and Structures, 18, 104026.

Ubertini, F., Gentile, C., and Materazzi, A. L. (2013). "Automated modal identification in operational conditions and its application to bridges." Engineering Structures, 46(0), 264 – 278.

Van Overschee, P. and De Moor, B. (1996). Subspace identification for linear systems: theory, implementation, applications. Kluwer Academic Publishers.

Wilkinson, A., Clemens, M., and Harding, V. (2004). "The effects of sebs-g-maleic anhydride reaction on the morphology and properties of polypropylene/pa6/sebs ternary blends." Polymer, 45(15), 5239–5249.

Yoda, R. (1998). "Elastomers for biomedical applications." Journal of Biomaterials Science, Polymer Edition, 9(6), 561–626.